ELSEVIER

Computers and Chemical Engineering 25 (2001) 313–322

Computers & Chemical Engineering

www.elsevier.com/locate/compchemeng

Dispersion and diffusion in coated tubes of arbitrary cross-section

Hugh M. Blackburn *

CSIRO Building Construction and Engineering, PO Box 56, Highett, Vic. 3190, Australia

Received 18 February 2000; received in revised form 13 November 2000; accepted 13 November 2000

Abstract

We examine a numerical technique developed to simulate unsteady dispersion and diffusion in coated tubes of arbitrary but axially-constant cross-section. The method is validated against analytical asymptotic solutions produced for tubes of circular section, then applied to the study of dispersion in equivalent tubes of square section, coated on one, two, three or four walls, and in a family of tubes of rectangular section, again with stationary phase coating on one wall. The results show that both the sectional geometry and coating regime have a profound influence on the axial dispersion, and hence on the efficiency of associated chromatography. For rectangular-sectioned columns with single-wall coating, the greatest separation efficiency results when the coating is applied to one of the longer segments of the cross-sectional perimeter. Published by Elsevier Science Ltd.

Keywords: Capillary; Chromatography; Dispersion; Separation

1. Introduction

The problem of transport of solute in a laminar flow within a coated tube of circular cross-section — a capillary separation column — was studied by Aris (1959), who provided analytical solutions for the time-asymptotic transport and dispersion rates. At the interface between the mobile solute phase and the stationary coating phase, Robin (or 'mixed') mass-transfer boundary conditions apply that result in coupling of unsteady transport in the two domains. The tendency towards unequal static partition of solute species between the two phases and the properties of the interphase coupling results in the separation of different solute species; various species are transported by the flow at different rates, as they spend differing average amounts of time in the stationary phase. The resulting separation of different species is the basis of capillary chromatography.

Following Aris (and the related contemporary work of Golay, 1958), there has been a number of analytical investigations (Davidson and Schroter, 1983; Purnama, 1988; Shankar and Lenhoff, 1991; Phillips and Kaye, 1998; Phillips, Kaye and Robinson, 1995) into different aspects of the problem; these have in the main concentrated on the behaviour in columns of circular section. Aris also provided a solution method for the case where both the tube and the coating are of arbitrary (but axially constant) section, with the restriction that one phase must completely surround the other; in topological terms, the outer, 'stationary', phase must be doubly connected, the inner, 'mobile', phase can be either simply or doubly connected. In order to remove these topological restrictions, and in order also to be able to study transient behaviour at small times, a numerical solution of the problem has been pursued here.

Motivation for the current work stems from a desire to study chromatography in columns of non-circular section, and with non-uniform coatings, such as might be produced by etching and spray coating. There is interest in columns of this kind for application in micro-scale ('on a chip') and high-performance liquid chromatography (HPLC) (e.g. Hudson et al., 1998; Spangler, 1998).

We analyse the physical problem and show that its numerical analogue produces a set of discrete Helmholtz equations that are coupled through Robin interphase boundary conditions. We demonstrate that the numerical method developed for the solution of the advection–diffusion problem successfully simulates the transport and dispersion of solute within a column of

* Tel.: +61-3-92526330; fax: +61-3-92526240.
E-mail address: hugh.blackburn@dbce.csiro.au (H.M. Blackburn).

0098-1354/01/$ - see front matter Published by Elsevier Science Ltd.
PII: S0098-1354(00)00658-X

circular section by comparison to Aris' analytical asymptotic results for tubes of circular section. These results are compared with those obtained for square and rectangular section columns.

2. Physical description

The separation column is decomposed into two domains, one for the mobile phase, and one for the stationary phase, as illustrated in Fig. 1. Inert carrier fluid flows within the mobile phase domain, and it is assumed that the transport of the solute has no effect on motion of the carrier. Flow of the carrier phase is assumed to be incompressible, which is the case for liquid carriers, and which is also a reasonable approximation for gases if simulation is carried out over a length of tube for which the pressure drop is minimal compared with the mean pressure. The tube diameter is assumed to be sufficiently large compared with the molecular mean free path that all species can be considered to be continua. The Reynolds number is low enough for the flow to be laminar.

The flow of carrier solute in the mobile phase domain is taken to be steady and invariant in the $\bar{z}$ direction (an overbar here denotes a dimensional variable), with velocity distribution $\bar{\omega}(\bar{x}, \bar{y})$ which can be found by solving a 2-D Poisson equation

$$\nabla^2\bar{\omega} = \frac{1}{\bar{\mu}}\left(-\frac{\mathrm{d}\bar{p}}{\mathrm{d}\bar{z}}\right) \quad \text{on } \Omega_\mathrm{m}, \tag{1}$$

where $\bar{p}$ is the pressure and $\bar{\mu}$ is the dynamic viscosity of the carrier phase. Given the applied pressure gradient and viscosity, Eq. (1) is solved for $\bar{\omega}$ in the (2-D) mobile phase section, Ω_m, with boundary condition $\bar{\omega} = 0$ at the wall (here, the Ω_m–Ω_s phase interface, Γ). For the method to be outlined in Section 3, this (numerical) solution is carried out as a preprocessing step prior to tackling the full advection–diffusion problem, and is used as data in its solution. For example, we show in Fig. 2 isopleths of the velocity distribution in tubes of circular, square and rectangular cross-section.

We will define a length scale $\bar{a} = \bar{A}_\mathrm{m}^{1/2}$, where $\bar{A}_\mathrm{m}$ is the cross-sectional area of the mobile phase domain. If $\bar{C}$ is the concentration of solute and $\bar{Q}$ its total amount, we define the dimensionless concentration $c = \bar{a}^3\bar{C}/\bar{Q}$. A convenient velocity scale is given by the average carrier velocity $\bar{W}$, from which we can derive a timescale $\bar{T} = \bar{a}/\bar{W}$.

It is convenient now to nondimensionalise the remaining variables and subsequent equations. The ratio of the cross-sectional area of the mobile phase to that of the stationary phase is defined as $\beta = \bar{A}_\mathrm{m}/\bar{A}_\mathrm{s}$. If the diffusion coefficients of solute in the mobile and stationary phases are, respectively, $\bar{D}_\mathrm{m}$ and $\bar{D}_\mathrm{s}$, we define their ratio $\lambda = \bar{D}_\mathrm{s}/\bar{D}_\mathrm{m}$. Using the mobile-phase diffusion coefficient we define the Péclet number,

$$Pe = \frac{\bar{W}\bar{a}}{\bar{D}_\mathrm{m}}. \tag{2}$$

At the mobile–stationary phase interface Γ there may be a surface resistance to mass transport, expressed through a mass-transfer coefficient $\bar{h}$. From this, we define a (mass-transfer) Nusselt number,

$$Nu = \frac{\bar{h}\bar{a}}{\bar{D}_\mathrm{m}}. \tag{3}$$

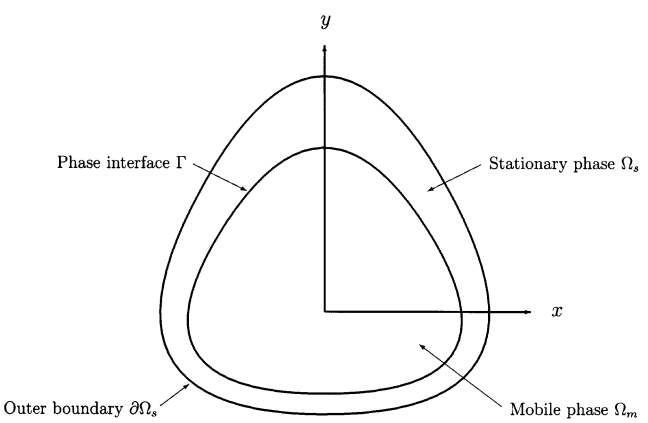

Fig. 1. Diagram showing the cross-section of a separation column of arbitrary shape; the column is uniform in the z (out-of-page) direction, which is the direction of solute phase flow.

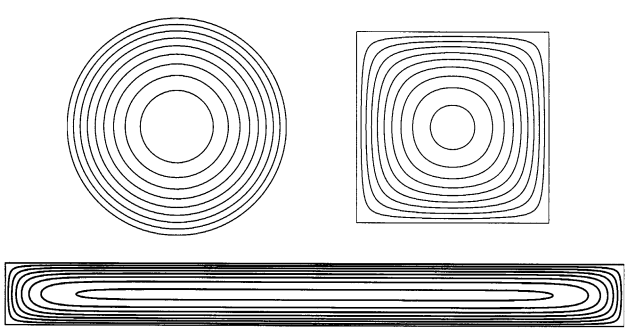

Fig. 2. Isopleths of mobile phase velocity w for laminar flow in tubes of circular, square and (10:1) rectangular cross-sections.

2.1. Transport equations

In the mobile phase, transport of c is governed by the unsteady advection–diffusion equation,

$$\frac{\partial c}{\partial t} + \omega\frac{\partial c}{\partial z} = \frac{1}{Pe}\nabla^2 c \quad \text{on } \Omega_\mathrm{m}, \tag{4}$$

while in the stationary phase, transport is governed by the unsteady diffusion equation,

$$\frac{\partial c}{\partial t} = \frac{\lambda}{Pe}\nabla^2 c \quad \text{on } \Omega_\mathrm{s}. \tag{5}$$

The outer wall of the column ($\partial\Omega_s$) is assumed inert and impervious to c, so the appropriate boundary condition to be applied at $\partial\Omega_s$ is zero flux, i.e. $\partial c/\partial n = 0$, where $\partial/\partial n$ is a derivative taken in the outward normal direction. To model a perfectly adsorbing boundary we could alternatively set $c = 0$. Where domain symmetry can be used to simplify the problem, the appropriate boundary condition is again specification of zero flux at the symmetry plane.

2.2. Boundary conditions at the phase interface

At the phase interface Γ, special boundary conditions must be applied. These have to account for the partition coefficient α, which expresses the equilibrium partition of concentration c between the stationary and mobile phases; $c_s = \alpha c_m$ in equilibrium. In addition, they have to account for equality of fluxes of c on each side of the interface, which in turn are proportional to the disequilibrium $c_s - \alpha c_m$. The appropriate conditions are (Aris, 1959).

$$\frac{\partial c_m}{\partial n} = -\lambda \frac{\partial c_s}{\partial n} = Nu(c_s - \alpha c_m), \tag{6}$$

where the directions of the unit outward normals, n, are equal and opposite at the interface Γ between Ω_m and Ω_s. Variation of the partition coefficient α between solute species is usually the primary determinant of species separation rates, but for low values of Nu the interface resistance can also have a significant effect.

The patching condition (Eq. (6)) can be rearranged to give a pair of Robin boundary conditions (Haberman, 1987) that are applied simultaneously in Ω_m and Ω_s:

$$\frac{\partial c_m}{\partial n} + Nu(\alpha c_m - c_s) = 0 \quad \text{on } \Omega_m,$$

$$\frac{\partial c_s}{\partial n} + \frac{Nu}{\lambda}(c_s - \alpha c_m) = 0 \quad \text{on } \Omega_s. \tag{7}$$

These have the generic form,

$$\frac{\partial c}{\partial n} + K(c - C) = 0. \tag{8}$$

2.3. Analytical asymptotic solutions

Aris (1959) provided detailed asymptotic solutions for the case in which the cross-sectional boundaries of all phases are concentric circles, with the mobile phase lying between radii $\bar{r}_0$ and $\bar{r}_1$, the stationary phase between $\bar{r}_1$ and $\bar{r}_2$. Using the 'method of moments', Aris was able to show that the location of the first axial moment (mean) of the concentration peak travels with asymptotic speed.

$$\bar{V} = \frac{\bar{W}_1(\bar{r}_1^2 - \bar{r}_0^2) + \bar{W}_2\alpha(\bar{r}_2^2 - \bar{r}_1^2)}{(\bar{r}_1^2 - \bar{r}_0^2) + \alpha(\bar{r}_2^2 - \bar{r}_1^2)}$$

where $\bar{W}_1$ is the mean velocity in the inner phase; $\bar{W}_2$ the mean velocity in the outer phase. In the usual case where $\bar{r}_0 = 0$ and $\bar{W}_2 = 0$, this reduces to the standard result:

$$\bar{V} = \frac{\bar{r}_1^2}{\bar{r}_1^2 + \alpha(\bar{r}_2^2 - \bar{r}_1^2)}\bar{W}_1 = \frac{1}{1+k}\bar{W} = R\bar{W}, \tag{9}$$

where k is the 'retention factor' α/β. The same asymptotic result is true regardless of the geometry of the cross-section.

Aris also provided equations for the asymptotic time rate of change of the higher axial moments of the (radially-integrated) concentration profile, for example of the variance $\bar{\sigma}^2$, i.e. the peak-broadening rate. Here Aris' (Eq. (17)) is simplified for the case, $r_0 = \bar{W}_2 = 0$, and written for the dimensionless variance $\sigma^2 = \bar{\sigma}^2/\bar{a}^2$.

$$\frac{Pe}{2}\frac{d\sigma^2}{dt} = R\left(1 + \frac{\kappa_1}{\pi}Pe^2\right) + (1-R)\left(\lambda + \frac{\kappa_2}{\pi}\frac{Pe^2}{\lambda\beta}\right) + R(1-R)^2\frac{1}{2\alpha\pi^{1/2}}\frac{Pe^2}{Nu}, \tag{10}$$

where, with $\rho = r_2/r_1$, the geometric factors,

$$\kappa_1 = \frac{1 + 6k + 11k^2}{48(1+k)^2},$$

$$\kappa_2 = \frac{2\rho^4 \ln\rho^2/(\rho^2-1) - 3\rho^2 + 1}{8(1+k)^2(\rho^2-1)}. \tag{11}$$

The numerical value of Eq. (10) gives the ratio of the asymptotic dispersion-induced axial spreading rate to the molecular diffusion rate in the mobile phase.

Aris derived a solution method for the asymptotic spreading rate in arbitrary cross-sections also (subject to the topological constraints mentioned in Section 1), leading to a generalisation of Eq. (10) that is cast in very similar form. By comparison of his two results, it may be seen that the first terms in the two bracketed expressions are related to diffusion in each phase, weighted by phase areas, and are otherwise independent of details of the flow and the geometry of cross-section. The factors κ_1 and κ_2 are controlled by the geometry of the cross-section, while the geometric dependence of the last term, which reflects resistance to mass transfer across the phase interface, relates only to its sectional perimeter length.

3. Numerical method

In order to convert the mathematical idealisation of the problem into one that can be solved numerically, we adopt a set of space–time discretisations of the governing PDEs. In what follows we present a particular discretisation based on backward differences in time, Fourier expansion in the axial direction, and spectral elements in the cross-sectional plane. This com-

bination provides exponential ('spectral') spatial convergence provided the solutions are smooth in each domain. Within the resolution regime tested here, the prime determinant of convergence is the tolerance adopted for iterative coupling between the stationary and mobile phases, to be described in Section 3.4. For additional detail concerning convergence properties, consult Blackburn (2000).

3.1. Fourier basis for axial coordinate direction

As the column is uniform in the axial (z) direction, it is convenient to assume that the problem is periodic in that direction, with periodic length L_z,

$$c(x, y, z, t) = c(x, y, z + L_z, t).$$

A slug of high concentration advected down the tube will seem to pass out one end and return through the other. Provided the axial length scale of the slug is always much shorter than the length of tube simulated, however, the results will be a good approximation of the actual transport.

With the assumption of periodicity, the 3-D scalar field c can be projected exactly onto a set of 2-D complex Fourier modes.

$$\hat{c}_k(x, y, t) = \frac{1}{L_z}\int_0^{L_z} c(x, y, z, t)e^{-i\phi kz}\,\mathrm{d}z \tag{12}$$

with the Fourier series reconstruction,

$$c(x, y, z, t) = \sum_{k=-\infty}^{+\infty} \hat{c}_k(x, y, t)e^{i\phi kz}, \tag{13}$$

where $i = (-1)^{1/2}$ and $\phi = 2\pi/L_z$. For numerical approximation, the set of modes is truncated at some finite number M; if the solution is smooth in the z-direction, the truncated approximation converges to the continuous solution exponentially fast (Gottlieb and Orszag, 1977). After Fourier transformation, the equivalents of the gradient and Laplacian operators become

$$\tilde{\nabla} \equiv \left(\frac{\partial}{\partial x}, \frac{\partial}{\partial y}, i\phi k\right),$$

$$\tilde{\nabla}^2 \equiv \left(\frac{\partial^2}{\partial x^2}, \frac{\partial^2}{\partial y^2}, -\phi^2 k^2\right) \equiv \tilde{\nabla}^2_{xy} - \phi^2 k^2$$

and transport equations (Eqs. (4) and (5)) become

$$\frac{\partial \hat{c}_k}{\partial t} + i\phi kw\hat{c}_k = \frac{1}{Pe}\tilde{\nabla}^2\hat{c}_k \quad \text{on } \Omega_\mathrm{m}, \tag{14}$$

$$\frac{\partial \hat{c}_k}{\partial t} = \frac{\lambda}{Pe}\tilde{\nabla}^2\hat{c}_k \quad \text{on } \Omega_\mathrm{s}, \tag{15}$$

for each Fourier mode k. Owing to the linearity of the original equations, Fourier transformation completely decouples the various modes, which can be evolved independently and/or concurrently. Thus the originally 3-D problem is converted into a set of 2-D problems.

3.2. Temporal evolution

A mixed explicit–implicit temporal evolution approximation is applied to the transformed transport equations; a fully implicit scheme could be implemented, but at the expense of requiring complex arithmetic. The temporal derivative of $\hat{c}_k$ is approximated at time level $n+1$ using a backward-differencing scheme of order J,

$$\frac{\partial \hat{c}_k^{(n+1)}}{\partial t} \approx \frac{1}{\Delta t}\left(\gamma_0\hat{c}_k^{(n+1)} + \sum_{q=0}^{J-1}\alpha_q\hat{c}_k^{(n-q)}\right), \tag{16}$$

while the advective terms are approximated at time level $n+1$ using polynomial extrapolation of order J.

$$i\phi kw\hat{c}_k^{(n+1)} \approx i\phi kw\sum_{q=0}^{J-1}\rho_q\hat{c}_k^{(n-q)}. \tag{17}$$

The discrete weights γ_0, α_q, ρ_q for schemes up to third order have been tabulated by Karniadakis, Israeli and Orszag (1991). Applying these approximations produces the following semi-discrete Helmholtz equations for the evolution of each Fourier mode.

$$\left(\tilde{\nabla}^2_{xy} - \phi^2k^2 - \frac{\gamma_0 Pe}{\Delta t}\right)\hat{c}_k^{(n+1)} = Pe\phi kw\sum_{q=0}^{J-1}\rho_q i\hat{c}_k^{(n-q)} + \frac{Pe}{\Delta t}\sum_{q=0}^{J-1}\alpha_q\hat{c}_k^{(n-q)} \quad \text{on } \Omega_\mathrm{m}, \tag{18}$$

$$\left(\tilde{\nabla}^2_{xy} - \phi^2k^2 - \frac{\gamma_0 Pe}{\lambda\Delta t}\right)\hat{c}_k^{(n+1)} = \frac{Pe}{\lambda\Delta t}\sum_{q=0}^{J-1}\alpha_q\hat{c}_k^{(n-q)} \quad \text{on } \Omega_\mathrm{s}, \tag{19}$$

or in generalised form,

$$(\tilde{\nabla}^2_{xy} - \xi_k^2)\hat{c}_k = \hat{f}_k. \tag{20}$$

At this stage the overall structure of the discrete problem is apparent: for every Fourier mode at each timestep there are two elliptic (Helmholtz) problems to be solved, coupled through Robin boundary conditions at the phase interface. In order to further define the discretisation we must adopt a numerical method for solution of these elliptic problems.

3.3. Galerkin spectral element method

To complete the discretisation, a Galerkin spectral element method is applied to the modal Helmholtz equations (Eq. (20)), as well as to the Poisson problem (Eq. (1)) for the velocity field w. To arrive at the Galerkin formulation, the partial differential equation is first multiplied by a weight or test function v and integrated over the domain, following which the integral is symmetrised by applying Gauss' theorem. This procedure results in the so-called weak form of the original equation. Applied to Eq. (20) this produces

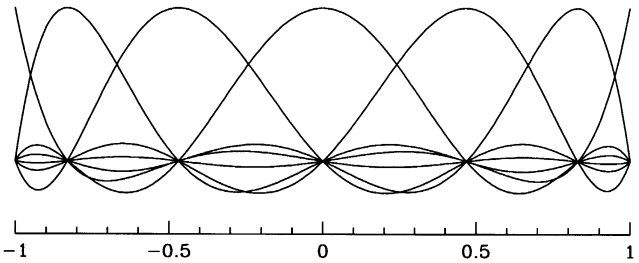

Fig. 3. One-dimensional Gauss–Lobatto–Legendre Lagrange basis functions on the master domain $[-1, 1]$ shown for a sixth order expansion.

$$\int_{\Omega}(\tilde{\nabla}_{xy}\hat{c}_k\tilde{\nabla}_{xy}v+\xi_k^2\hat{c}_kv)\mathrm{d}\Omega=-\int_{\Omega}\hat{f}_kv\ \mathrm{d}\Omega+\int_{\Gamma}\frac{\partial\hat{c}_k}{\partial n}v\ \mathrm{d}\Gamma, \tag{21}$$

where Ω is either Ω_m or Ω_s, and Γ represents any boundary on which $\hat{c}_k$ is not directly specified, i.e. all boundaries in the present problem. One means of accommodating Robin boundary conditions (Eq. (8)) on Γ is to insert them into the last term in Eq. (21), and then to rearrange the result to give

$$\int_{\Omega}(\tilde{\nabla}_{xy}\hat{c}_k\tilde{\nabla}_{xy}v+\xi_k^2\hat{c}_kv)\mathrm{d}\Omega+\int_{\Gamma}K\hat{c}_kv\ \mathrm{d}\Gamma$$
$$=-\int_{\Omega}\hat{f}_kv\ \mathrm{d}\Omega+\int_{\Gamma}KCv\ \mathrm{d}\Gamma. \tag{22}$$

A Galerkin problem results when the function space from which trial functions $\hat{c}_k$ and test functions v are drawn is the same. This must be a Sobolev-1 space for Eq. (22) to be guaranteed convergence (Strang and Fix, 1973). For discrete solution a finite number of functions are chosen, leading to a system of algebraic equations. For solution in complex geometries, the domain is subdivided into a set of simpler geometries (finite elements), with the test and trial functions having compact support over adjoining elements. Typically the integrals in Eq. (22) are approximated numerically using an appropriate Gauss rule.

The method is further defined by choosing a function space from which the finite element test and trial functions are drawn. The conventional finite element method uses functions which are typically low-order polynomials, however, we have chosen instead a high-order method. The spectral element method (Patera, 1984; Karniadakis and Sherwin, 1999) is related to the conventional finite element method but employs Lagrange basis functions that have the Gauss–Lobatto–Legendre (GLL) points as knots. For problems with smooth solutions, the spectral element method generates approximations that converge exponentially to the true solution as the polynomial order in each element is increased (Maday and Patera, 1989). The expansion basis on each element is an isoparametric mapping of tensor-products of 1-D GLL Lagrange interpolants of arbitrary order (see Fig. 3 for a sixth order expansion).

3.4. Iterative coupling

Previously published techniques developed for inter-domain coupling in elliptic problems discussed by Quarteroni and Valli (1999) are designed for the case where there is a single global problem (e.g. with identical mechanical properties in each sub-domain) and also are not directly applicable for domains coupled through Robin boundary conditions. We have thus developed a simple iterative coupling of solutions in the two domains (Blackburn, 2000). It is interesting that the method relies on the linkage provided by a finite value of the interface mass-transfer coefficient, a physical effect sometimes ignored in analytical treatments.

In each sub-domain only the values of c from the other side of the interface are treated as data supplied by the previous iteration (here the index p relates to a sub-iteration that is distinct from the timestep).

$$\frac{\partial c_\mathrm{m}^{(p)}}{\partial n}=Nu(c_\mathrm{s}^{(p-1)}-\alpha c_\mathrm{m}^{(p)})\quad\text{on }\Omega_\mathrm{m},$$
$$\frac{\partial c_\mathrm{s}^{(p)}}{\partial n}=\frac{Nu}{\lambda}(\alpha c_\mathrm{m}^{(p-1)}-c_\mathrm{s}^{(p)})\quad\text{on }\Omega_\mathrm{s}. \tag{23}$$

As dictated by Eq. (22), the values at step (p) are interpreted as contributing to the system Helmholtz matrix, while those at $(p-1)$ contribute to the forcing. This iteration technique was found to be convergent, and may be combined with iterative solution of the elliptic problem. Iteration continues until the relative change in the L_2-norm of the solution in each domain drops below a fixed tolerance ϵ; typically here $\epsilon=1\times10^{-10}$. The method can be generalised to deal with an arbitrary number of stationary phases.

4. Column with circular cross-section

In order to test the numerical method developed for the coupled advection–diffusion problem, the computed asymptotic time rate of change of the location and spread of the concentration peak compared with the analytical results (Eqs. (9) and (10)) for one set of parameters in a column of circular section. Parameters were $Pe=Nu=\alpha=10$; $\beta=50$; $\lambda=250\times10^{-6}$. The retention factor $k=0.2$, while the geometric parameters $\kappa_1=0.03894$, $\kappa_2\approx0.0115166$. Spectral element meshes for the two domains are illustrated in Fig. 4; symmetry properties allow only a quarter of the domain to be represented. Spectral element shape functions were ninth order tensor-product GLL Lagrange interpolants, and 64 planes or 32 complex Fourier modes of data were employed in the column-axis direction. Column length $L_z=1000$, and a Gaussian-shaped initial concentration in the mobile phase with axial variance $\sigma^2=800$ was employed. The Gaussian initial pulse is a numeri-

cally convenient shape, and relatively undemanding in terms of axial resolution, as it is smooth in both physical and Fourier domains; however, the method would work with any arbitrary initial distribution given sufficient resolution, since physical diffusion will rapidly act to overcome any discontinuities. Time integration was second order ($J=2$) with $\Delta t=0.1$.

Profiles of tube centreline concentration are shown in Fig. 5 starting at the initial condition, then at five times up to $t=500$. The decline from the initial peak is brought about by a combination of radial equilibration and partition between phases of the initially Gaussian-shaped concentration pulse. The effects of domain periodicity may be just observed for the final profile. Clearly the partition between phases has the expected effect of slowing the mean transport rate; without the retarding effect of the wall coating, the concentration peak would have been centred at $z=1000$ when $t=500$.

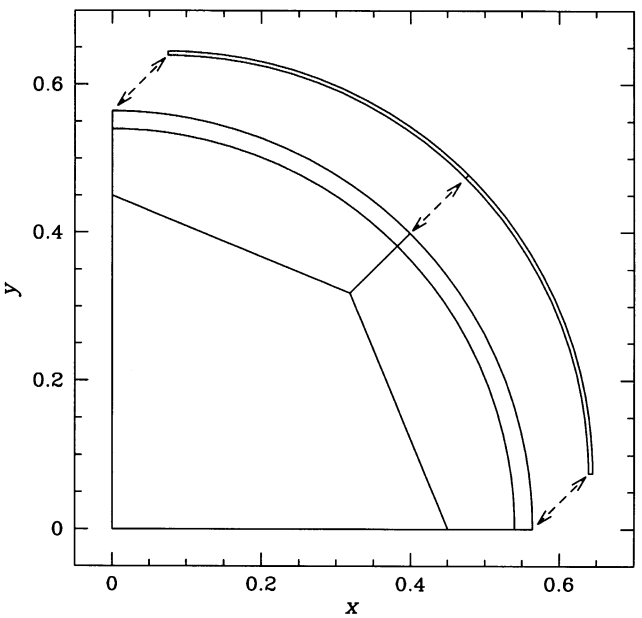

Fig. 4. Two-domain spectral element mesh for simulation of transport in a separation column of circular section. There are five elements in the mobile phase and two in the stationary phase — the two phases are shown separated for clarity.

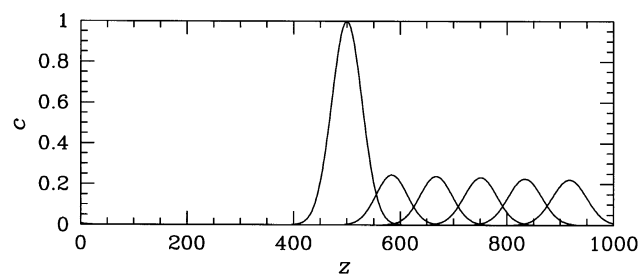

Fig. 5. Tube centreline concentration profiles for flow in a column of circular cross-section. Profiles are for times $t=0$, 100, 200, 300, 400 and 500.

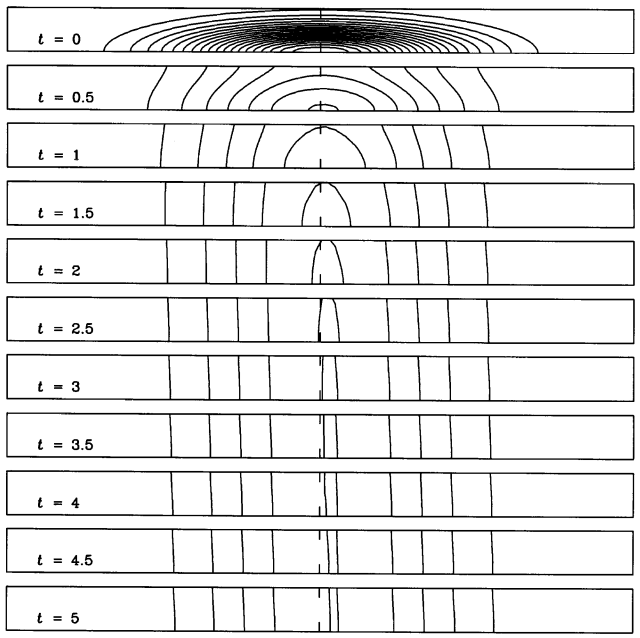

Fig. 6. Contours of c in the mobile phase near the initial position of the concentration pulse at early times for the circular-section column. In each plot, the lower boundary corresponds to the column centreline, and the upper boundary to the phase interface Γ.

The mean and variance of the concentration profiles are approximated numerically as

$$\mu=\frac{\int_0^{L_z} zC(z)\mathrm{d}z}{\int_0^{L_z} C(z)\mathrm{d}z}\approx\frac{\sum_{j=0}^{N_z-1} z_j C_j}{\sum_{j=0}^{N_z-1} C_j}, \tag{24}$$

$$\sigma^2=\frac{\int_0^{L_z} (z-\mu)^2 C(z)\mathrm{d}z}{\int_0^{L_z} C(z)\mathrm{d}z}\approx\frac{\sum_{j=0}^{N_z-1} (z_j-\mu)^2 C_j}{\sum_{j=0}^{N_z-1} C_j}, \tag{25}$$

where N_z is the number of axial planes and $C(z)=\int_{\Omega_\mathrm{m}} c(z)\mathrm{d}\Omega$ is the cross-sectional integral of c at location z, computed using Gauss–Lobatto quadrature. Higher moments of the concentration profile may be similarly approximated.

The analytic expressions (Eqs. (9) and (10)) for the asymptotic time rates of change $\mathrm{d}\mu/\mathrm{d}t=R=0.8\bar{3}$, $Pe\ \mathrm{d}\sigma^2/2\ \mathrm{d}t\approx(1.846472+0.4888240+0.00652997)=2.3418264$. In order to obtain approximately asymptotic values from the simulation, time integration was carried out up until $t=500$, then from tabulated estimates of μ and σ^2, finite differences over the final interval of $\Delta t=200$ were used to estimate $\mathrm{d}\mu/\mathrm{d}t\approx 0.83333244$ and $Pe\ \mathrm{d}\sigma^2/2\ \mathrm{d}t\approx 2.3418266$, showing very good agreement to the analytical solutions.

The initial condition for the simulation is a 3-D Gaussian-shaped pulse of c, centred in the mobile phase. Contours of concentration, shown in Fig. 6, demonstrate how the shape of the pulse redevelops towards its asymptotic shape as dispersion, diffusion and phase partition take effect.

Conservation of c as the partition between phases becomes established is illustrated for early times in Fig. 7, where the total amount of c in each phase (normalised by the initial amount in the mobile phase at $t = 0$), Σ, is shown as a function of time. In the mobile phase, the asymptotic value of $\Sigma_m = R$, while for the stationary phase the asymptotic value of $\Sigma_s = 1 - R$.

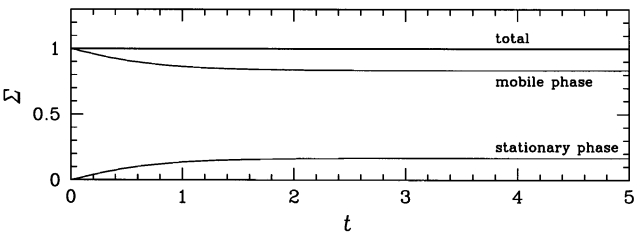

Fig. 7. Partition of c between phases at early times, illustrating conservation of mass. For each phase, Σ is the volume integral of c, normalised by the value existing in the mobile phase at $t = 0$.

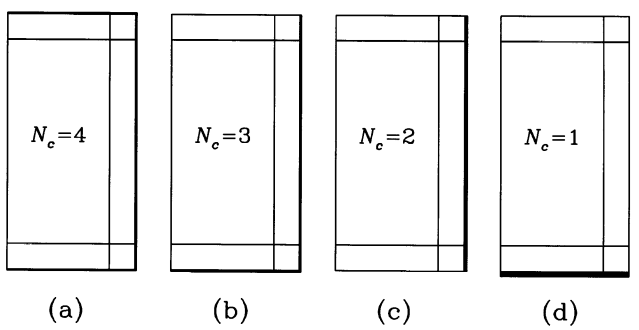

Fig. 8. Meshes for simulations with square cross-sections, (a) coated on four walls, $N_c = 4$; (b) coated on 3 walls, $N_c = 3$; (c) coated on two walls, $N_c = 2$; (d) coated on one wall, $N_c = 1$. Sections are symmetric about vertical centrelines; only half of the square is represented.

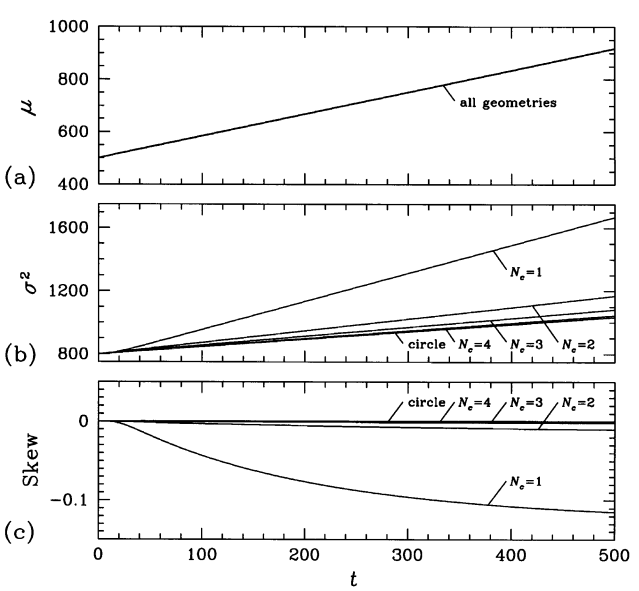

Fig. 9. Simulation results showing first three axial moments in mobile phase domain of solute pulse as functions of time for circular section compared with those for square sections coated on four ($N_c = 4$), three ($N_c = 3$), two ($N_c = 2$) and one ($N_c = 1$) walls.

5. Columns with square cross-sections

The starting point for this work was a desire to study performance of chromatography in columns of non-circular section and with arbitrary coating geometry. We now turn to comparing the dispersion performance of the circular section dealt with in Section 4 to that for a family of square sections, which have identical dimensionless parameters to the circular section but which vary in coating geometry. Specifically, we examine the dispersion in four square-sectioned columns that are coated on four, three, two and one walls ($N_c = 4$, 3, 2 and 1 respectively).

Meshes for the four square-sectioned columns are shown in Fig. 8. Note that the property of symmetry about vertical centrelines has been assumed. The meshes differ only in the geometry of the coating regime, and in the boundary conditions applied on the outer edges of the mobile phase. As indicated above, the thickness of the stationary phase has been adjusted in each case in order to maintain $\beta = 50$, and since the partition coefficient α was maintained constant, the retention factor k is the same for all columns.

Simulation results, presented in terms of the time evolution of the first three axial moments of the solute pulse distribution in Ω_m for the four square cross-sectioned columns, are shown in Fig. 9 — results for the circular-section column are shown for comparison. Since the retention factor k is identical for all these columns, it is expected that the asymptotic transport rates for the mean (μ) would be identical, as is borne out by the results presented in Fig. 9a; asymptotic transport rates agree with the theoretical value to at least five significant figures for all cases. The initial mean location, $\mu = 500$, corresponds to the pulse being centred in the domain ($L_z = 1000$) at $t = 0$.

For chromatography applications, it is the spreading rate of the peak that determines the separation efficiency of the column, and it can be seen in Fig. 9b that the coating regime has a substantial effect. While the spreading rate for $N_c = 4$ is effectively the same as for the column with circular section, performance deteriorates as the number of coated walls reduces. The asymptotic spreading rate, $d\sigma^2/dt$, for $N_c = 1$ is greater than that for the circular-section column by a factor of

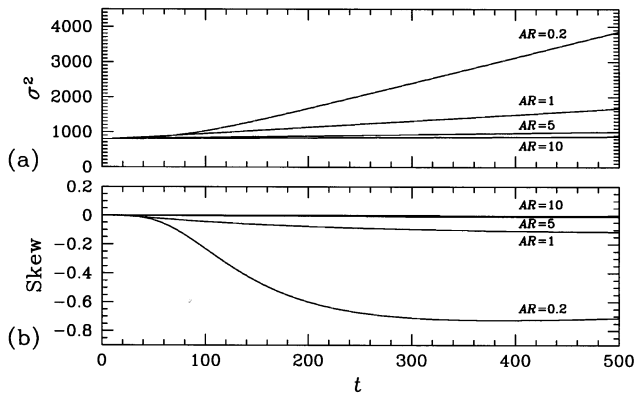

Fig. 10. Simulation results showing axial variance and skewness in mobile phase domain of solute pulse as functions of time for rectangular section columns that have stationary phase coating on one wall, and nominated aspect ratios AR.

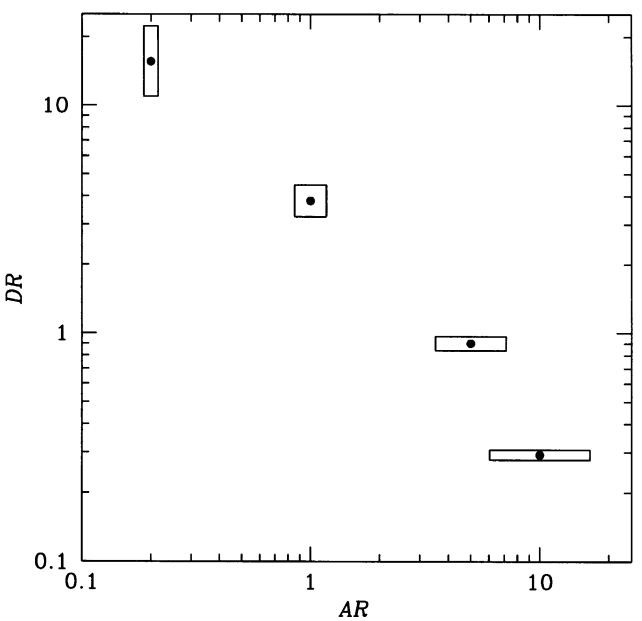

Fig. 11. Simulation results showing DR, the ratio of the asymptotic rate of change of the axial variance of the solute pulse normalised by the value for a column of circular cross-section, as a function of the rectangular cross-section aspect ratio AR, when there is a stationary phase coating on a single side of the rectangle. Rectangles drawn centred on the data points indicate the cross-section geometry for each AR; in each case the coating would be on one of the horizontal faces.

approximately 3.8 — the overall effective axial diffusion rate for $N_c = 1$ is almost nine times higher than the molecular diffusion of the solute in the stagnant carrier. The effect of coating regime on the axial skewness of the distribution at short times is also substantial, as can be seen in Fig. 9c, however, the skewness will approach zero asymptotically (Aris, 1959).

6. Columns with rectangular cross-sections

In order to examine the effect of cross-section shape on dispersion, simulations were carried out for rectangular cross-section columns, with a stationary phase coating only on one wall (the square section $N_c = 1$ from Section 5 is one of the family of sections examined). The variable here was the aspect ratio AR of the section, where this is defined as the ratio of sectional perimeter length of the coated wall to that of an adjacent wall. Other dimensionless parameters were maintained the same as for the previous simulations, and in particular the sectional length scale $\bar{a}$ is still based on the area of the mobile phase cross-section. The results are presented in Fig. 10, where rates of change for the axial variance and skewness of the solute pulse for different values of AR are compared.

The aspect ratio AR of the rectangular section is seen to have a very substantial effect on the axial dispersion rate. In Fig. 11 the asymptotic time rate of change of the axial variance of the solute pulse normalised by the value for the circular cross-section, DR, is shown as a function of the rectangle aspect ratio AR. The value 'dispersion ratio' (DR) represents the effective axial diffusion rate of a solute pulse compared with what would be observed in an equivalent conventional circular coated tube. Evidently the separation efficiency of the singly-coated rectangular section exceeds that for the circular section (i.e. $DR < 1$) for $AR > 5$, approximately, given the set of dimensionless parameters adopted for the simulations. Conversely, low aspect ratios can produce columns of comparatively poor separation efficiency ($DR \gg 1$ when $AR \ll 1$).

The process of redistribution of c from the initial condition in the $AR = 0.2$ column is shown in Fig. 12. Even at $t = 5$ the front-to-rear asymmetry that produces the comparatively high negative values of skewness in Fig. 10b can be observed.

7. Discussion and conclusions

Starting from physical fundamentals, a numerical simulation method has been developed for simulation of diffusion and dispersion in capillary chromatography. The method incorporates a new iterative technique for domain decomposition coupled across a phase interface through Robin boundary conditions. Results demonstrate the success of the method, and its potential application to prediction of mean transport and peak-broadening rates in capillary separation, as well as early-time evolution from initial conditions.

Comparative simulations with different cross-sectional geometries but with matching dimensionless parameters illustrate that variations in coating regime and cross-section shape both play an important role in

influencing axial dispersion rates. Comparing results for a column with a circular cross-section to those for a square cross-section, but with stationary phase coating on all four walls showed that the axial dispersion rates were virtually identical for the parameter set selected for simulation. Changing the coating in the square cross-section column to a single coated wall produced a marked increase in axial dispersion rate. For rectangular-section columns with coating on one wall, the aspect ratio of the rectangle had a substantial effect on axial dispersion rates, with higher aspect ratios producing lower axial dispersion, other factors equal — axial dispersion rates significantly lower than for an equivalent circular-section column can be achieved.

The numerical method we have outlined is not dependent on the adoption of Fourier expansions and spectral elements; other combinations of discretisations should also work. See Henderson (1999) for an analysis of operation counts for the spectral element methods used here. The iterative coupling across the phase interface (Section 3.4) could benefit from a more sophisticated approach, as the convergence rate of this coupling is a prime determinant of run-time at present. Typically, of the order of 100 iterations are required per time step to achieve the convergence tolerance $\epsilon = 1 \times 10^{-10}$, when this iteration is uncoupled from the Helmholtz solutions (Section 3.3) on each domain.

The amount of time required for solution is not heavily dependent on the shape of the domain. For example, the 5000-step simulations used to produce Fig. 9 required 44.5 h for the circular-section mesh shown in Fig. 4, and 45.5 h for the single-coating square-section mesh shown in Fig. 8d, when run on a 175 MHz SGI R10000 workstation — these simulation results are comparable since the meshes have similar numbers of elements in each phase, and the same resolution. Simulations for the mesh shown in Fig. 8a, with three times as many elements in the stationary phase, and approximately twice as many elements in total than the mesh in Fig. 4, take approximately twice as long.

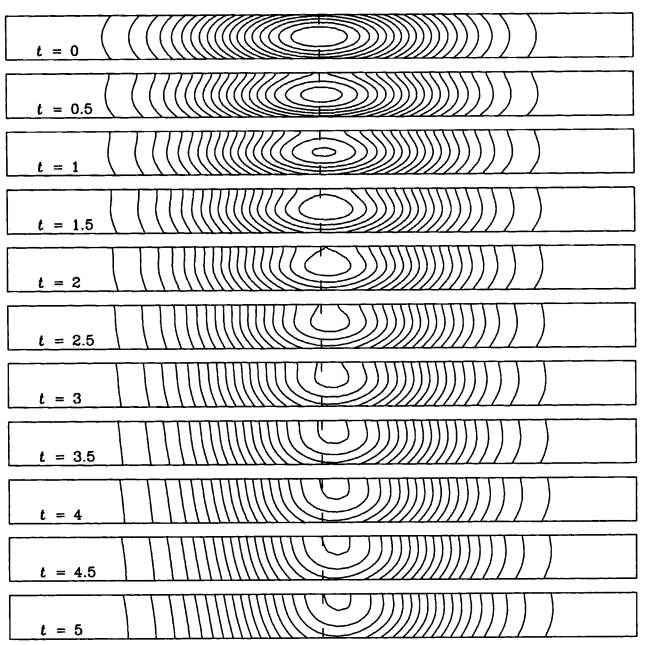

Fig. 12. Contours of c in the mobile phase near the initial position of the concentration pulse at early times on the centreplane of the 1:5 aspect ratio rectangular section ($AR = 0.2$). In each plot, the lower boundary corresponds to the phase interface Γ, and the upper boundary to a solid wall.

It is significant that the separation performance of a column can be substantially improved by changing the aspect ratio of its cross-section, however, the improved performance comes at the cost of requiring a higher pressure drop for a given volumetric flow rate, given a constant cross-sectional area. For example, the pressure gradient required to drive a laminar flow of carrier through a 10:1 aspect ratio rectangular-section tube is 5.1 times greater than is required for the same volumetric flow rate through a circular-section tube of the same area (a square section requires a pressure gradient that is only 13% greater than a circular one).

The physical explanation for the changes in separation performance with coating regime and geometry is probably related to the change in thickness of the stationary phase and available mass-transport area at the interface of the two phases. This is an inference that can be drawn from Fig. 9: for the square-section tubes there, the thickness of the stationary phase increases as the number of coated sides, N_c, reduces from 4 to 1, with a consequent increase in spreading rate. The thickness of the stationary phase is not the sole determinant of the effect, however; for example in Fig. 11 the coating thickness for the rectangular tube with AR = 10 is approximately 12% circular tube, the perimeter length of the interface Γ lower by the same amount, but the dispersion ratio DR is approximately 70% less. This indicates that a characteristic cross-flow length of diffusion is also significant in influencing dispersion: for example an integral-weighted minimum length from Γ to an isopleth of average velocity.

Acknowledgements

This work was supported in part by AusIndustry R & D Start grant GRA 00621.

References

Aris, R. (1959). On the dispersion of a solute by diffusion, convection and exchange between phases. *Philosophical Transactions of The Royal Society of London A*, *252*, 538–550.

Blackburn, H. M. (2000). Domain decomposition with Robin boundary conditions across a phase interface. *ANZIAM Journal*, *42*(E), 258–285 See http://anziamj.austms.org.au/-V42/CTAC99/Blac.

Davidson, M. R., & Schroter, R. C. (1983). A theoretical model of adsorption of gases by the bronchial wall. *Journal of Fluid Mechanics*, *129*, 313–335.

Golay, M. J. E. (1958). Theory of chromatography in open and coated tubular columns with round and rectangular cross-sections. In D. H. Desty, *Gas chromatography 1958* (pp. 36–53). London: Butterworths.

Gottlieb, D., & Orszag, S. A. (1977). *Numerical analysis of spectral methods: theory and applications*. SIAM.

Haberman, R. (1987). *Elementary applied partial differential equations* (second ed.). Englewood Cliffs, NJ: Prentice-Hall.

Henderson, R. D. (1999). Adaptive spectral element methods for turbulence and transition. In T. J. Barth, & H. Deconinck, *High-order methods for computational physics* (pp. 225–324). Berlin: Springer.

Hudson, M. L., Kottenstette, R., Matzke, C. M., Frye-Mason, G. C., Shollenberger, K. A., Adkins, D. R., & Wong, C. C. (1998). Design, testing, and simulation of microscale gas chromatography columns. In *Micro-electro-mechanical systems* (pp. 207–214). ASME.

Karniadakis, G. E., & Sherwin, S. J. (1999). *Spectral/hp element methods for CFD*. Oxford: Oxford University Press.

Karniadakis, G. E., Israeli, M., & Orszag, S. A. (1991). High-order splitting methods for the incompressible Navier–Stokes equations. *Journal of Computer and Physics*, *97*(2), 414–443.

Maday, Y., & Patera, A. T. (1989). Spectral element methods for the incompressible Navier–Stokes equations. In A. K. Noor, & J. T. Oden, *State-of-the-art surveys on computational mechanics* (pp. 71–143). ASME.

Patera, A. T. (1984). A spectral element method for fluid dynamics: laminar flow in a channel expansion. *Journal of Computer and Physics*, *54*, 468–488.

Phillips, C. G., & Kaye, S. R. (1998). Approximate solutions for developing shear dispersion with exchange between phases. *Journal of Fluid Mechanics*, *374*, 195–219.

Phillips, C. G., Kaye, S. R., & Robinson, C. D. (1995). Time-dependent transport by convection and diffusion with exchange between two phases. *Journal of Fluid Mechanics*, *297*, 373–401.

Purnama, A. (1988). Boundary retention effects upon contaminant dispersion in parallel shear flows. *Journal of Fluid Mechanics*, *195*, 393–412.

Quarteroni, A., & Valli, A. (1999). *Domain decomposition methods for partial differential equations*. Oxford: Oxford Science Publications.

Shankar, A., & Lenhoff, A. M. (1991). Dispersion and partitioning in short coated tubes. *Ind. Eng. Chem. Res.*, *30*, 828–835.

Spangler, G. E. (1998). Modification of Golay's theory for rectangular microfabricated gas chromatograph columns. In *Micro-electro-mechanical systems* (pp. 215–222). ASME.

Strang, G., & Fix, G. J. (1973). *An analysis of the finite element method*. Englewood Cliffs, NJ: Prentice-Hall.